The Astrophysical Journal, 591:1075–1085, 2003 July 10

THE EVOLUTION OF A STRUCTURED RELATIVISTIC JET AND GAMMA-RAY BURST AFTERGLOW LIGHT CURVES

Pawan Kumar
Department of Astronomy, University of Texas, Austin, TX 78731; pk@astro.as.utexas.edu

and

Jonathan Granot
Institute for Advanced Study, Princeton, NJ 08540; granot@ias.edu
Received 2002 November 13; accepted 2003 March 3

ABSTRACT

We carry out a numerical hydrodynamical modeling for the evolution of a relativistic collimated outflow as it interacts with the surrounding medium and calculate the light curve resulting from synchrotron emission of the shocked fluid. The hydrodynamic equations are reduced to one-dimensional by assuming axial symmetry and integrating over the radial profile of the flow, thus considerably reducing the computation time. We present results for a number of different initial jet structures, including several different power laws and a Gaussian profile for the dependence of the energy per unit solid angle, ϵ, and the Lorentz factor, Γ, on the angle from the jet symmetry axis. Our choice of parameters for the various calculations is motivated by the current knowledge of relativistic outflows from gamma-ray bursts and the observed afterglow light curves. Comparison of the light curves for different jet profiles with gamma-ray burst afterglow observations provides constraints on the jet structure. One of the main results we find is that the transverse fluid velocity in the comoving frame (v_t) and the speed of sideways expansion for smooth jet profiles is typically much smaller than the speed of sound (c_s) throughout much of the evolution of the jet; v_t approaches c_s when Γ along the jet axis becomes of order a few (for a large angular gradient of ϵ, $v_t \sim c_s$ while Γ is still large). This result suggests that the dynamics of relativistic structured jets may be reasonably described by a simple analytic model in which ϵ is independent of time, as long as Γ along the jet axis is larger than a few.

Subject headings: gamma rays: bursts — gamma rays: theory

1. INTRODUCTION

The great advance in our understanding of gamma-ray bursts (GRBs) in the last 5 years has largely resulted from the observation and modeling of afterglow radiation—emission observed for days to months after the end of a GRB, in the X-ray, optical, and radio bands. The basic procedure for obtaining information about the explosion, such as the energy release, opening angle of the emergent jet, the density of the medium in the immediate vicinity of the GRB, etc., is that of comparing the observed afterglow light curve with the theoretically calculated flux (Wijers & Galama 1999; Granot, Piran, & Sari 1999b; Chevalier & Li 2000; Panaitescu & Kumar 2001a, 2001b, 2002). Most works on GRB jets assume a homogeneous (or top-hat) jet, in which all the hydrodynamic quantities of the jet, such as its Lorentz factor and energy density, are the same within some finite well-defined opening angle around the jet axis and drop to zero at larger angles (e.g., Piran 1999, 2000).

A comparison of theoretically calculated light curves, under several simplifying assumptions described below (and assuming a top-hat jet), with observed light curves in X-ray, optical, and radio bands for eight GRBs has led to a number of interesting results (Panaitescu & Kumar 2001b). Perhaps the most remarkable discovery is that the kinetic energy in the relativistic outflow is nearly the same, within a factor of 5, for the set of eight GRBs. A similar result has been obtained by Piran et al. (2001) through a method that requires fewer assumptions. Frail et al. (2001) have also found that the energy radiated in GRBs does not vary much from one burst to another. The opening angle for GRB jets is found to be in the range 2°–20°, and the density of the external medium in the vicinity of GRBs is estimated to be between 10^{-3} and 30 cm^{-3}. Moreover, there is no firm evidence for the density to vary inversely as the square of the distance in all but one case (Price et al. 2002; Panaitescu & Kumar 2002), which is surprising in light of the currently popular model for GRBs, the collapsar model. In the competing supranova model, the roughly constant density profiles that are inferred from fits to observations may arise naturally (Königl, & Granot 2002).

The possibility that GRB jets can display an angular structure, i.e., that the Lorentz factor, γ, and energy per unit solid angle, ϵ, in the GRB outflow can vary smoothly as power laws in the angle θ from the jet axis, was proposed by Mészáros, Rees, & Wijers (1998). Recently, in view of the evidence described above for a roughly constant energy in the gamma-ray emission and in the kinetic energy of the afterglow shock, it has been suggested that GRB jets might have a universal structure, and the differences in the observed properties of GRBs and their afterglows arise because of different viewing angles, $\theta_{\rm obs}$, with respect to the jet axis (Lipunov, Postnov, & Prokhorov 2001; Rossi, Lazzati, & Rees 2002; Zhang & Mészáros 2002). In this interpretation, the jet break in the light curve occurs when the Lorentz factor along the line of sight, $\gamma(\theta_{\rm obs})$, drops to $\sim \theta_{\rm obs}^{-1}$, so that the jet break time, t_j, is determined by the viewing angle, $\theta_{\rm obs}$, rather than by the opening angle of the top-hat jet, as in the conventional interpretation.

The calculation of light curves from a shock-heated, collimated, relativistic outflow has been carried out by a few research groups (Rhoads 1999; Panaitescu & Mészáros 1999; Kumar & Panaitescu 2000; Moderski, Sikora, & Bulik 2000; Granot et al. 2002). However, most of the works to

date have been based on a simplified model for the jet dynamics and on a number of ad hoc assumptions. All the above works assume a top-hat jet, and furthermore, most of them model the dynamics of the jet at times much greater than the deceleration time as uniform expansion at the sound speed or the speed of light (in the local rest frame of the shocked fluid)—the results are nearly the same for both of these cases. Similar simplifications were made in the recent work on a universal structured jet (Rossi et al. 2002). An exception to this is the work of Granot et al. (2001), in which the dynamics of an initial top-hat jet was calculated using a hydrodynamic simulation, and the resulting light curves were calculated numerically. However, such hydrodynamic simulations are very time consuming and difficult to apply to a structured jet, so that there is currently no rigorous treatment of the hydrodynamic evolution of a structured jet. In this paper we develop such a rigorous treatment for the dynamics of structured jets, which at the same time is not very time consuming and may become practical to include in fits to afterglow observations.

Another simplification made in previous works (including all the works mentioned above) for lack of a better alternative, is also made in this work, namely, that the strength of the magnetic field and the energy in the electrons are determined by assuming that the energy densities of the magnetic field and of the electrons are constant fractions of the internal energy density of the shocked fluid. It is unclear how some of the simplifying assumptions in the afterglow light-curve modeling affect the overall burst parameters and properties we have inferred as described above.

Some progress has been made recently toward understanding the generation of magnetic fields in relativistic collisionless shocks: the numerical simulations of M. V. Medvedev (2002)[1] show that magnetic fields generated behind collisionless relativistic shocks via the Weibel instability (Medvedev & Loeb 1999) do not decay to very low values within a short distance behind the shock, as was previously thought (Gruzinov 1999, 2001) but rather approach a finite value in the bulk of the shocked fluid behind the shock, which might be compatible with the values inferred from afterglow observations. Moreover, the modeling of GRB afterglow light curves indicates that the energy fraction in electrons is close to equipartition (Panaitescu & Kumar 2001b), hence the parameterization of electron energy does not appear to be a serious drawback for current models. Thus, at present, one of the biggest uncertainties in the afterglow modeling is the assumption of a uniform jet and the simplified jet dynamics. The purpose of this paper is to remedy this situation and develop a much more realistic model for GRB jets. Fitting afterglow observations with light curves that are calculated using a realistic jet model and dynamics may both constrain the structure of GRB jets (the initial distribution of the Lorentz factor and energy per unit solid angle as a function of the angle from the jet axis) and provide more accurate estimates for the physical parameters, which include the external density profile and the parameters describing the microphysics of relativistic collisionless shocks.

In the next section (§ 2) we discuss the evolution of structured jets. In § 2.1 we describe our hydrodynamical scheme, in which we begin from the full hydrodynamic equations, assume axial symmetry, and integrate over the radial structure, thus reducing the problem to a set of one-dimensional partial differential equations that are solved numerically. The initial and boundary conditions are outlined in § 2.2, while results for some physically interesting cases are shown in § 2.3. In § 3 we describe the light curve calculation and compare the results of hydrodynamical simulations with a simplified model. The main results are summarized in § 4.

[1] See http://cfa-www.harvard.edu/grbconf/.

2. JET MODELING

We begin with a brief description of the uniform jet model, and then we describe in some detail the evolution of a more realistic, structured jet and the afterglow light curves resulting from emission by the shock-heated medium swept up by the jet. Most calculations of GRB light curves have assumed that the properties of the relativistic outflow do not vary across the jet and that the jet dynamics is described by a uniform lateral expansion in the comoving frame, at close to the speed of sound, c_s, which for a hot relativistic plasma is $3^{-1/2}$ times the speed of light, c. These assumptions drastically simplify the calculation of the evolution of the jet opening angle, θ_j, with time: the increase in the lateral size of the jet in comoving time $\delta t_{\rm co}$ is $c_s \delta t_{\rm co}$, and so the change to its angular size is $\delta\theta_j = c_s \delta t_{\rm co}/r = (c_s/c)\delta r/(r\gamma)$ or

$$\frac{d\theta_j}{dr} = \frac{c_s}{c\gamma r} \ .$$

This equation, together with the energy conservation equation, describes the dynamics of a uniform relativistic disk or a jet. This equation implies that the jet opening angle θ_j starts to increase when γ drops below θ_j^{-1}, and from that time onward the jet opening angle is roughly γ^{-1}. A detailed discussion of the uniform jet dynamics and light-curve calculation can be found in a number of papers (e.g., Rhoads 1999; Panaitescu & Mészáros 1999; Sari, Piran, & Halpern 1999; Kumar & Panaitescu 2000). Such a uniform jet with sharp well-defined edges shall be referred to as a top-hat jet.

However, two-dimensional hydrodynamic simulations of the evolution of a jet that is initially uniform within some finite opening angle (Granot et al. 2001) have shown that the lateral expansion of the jet is smaller than that predicted by the simple models described above. This suggests that the assumption of lateral expansion at close to the sound speed in the comoving frame, which is made in most simple jet models, is not valid. Nevertheless, the light curves calculated from these simulations show a sharp jet break in the light curves, similar to that seen in most afterglow observations, around the time γ drops to θ_j^{-1}.

2.1. *Dynamics of Structured Relativistic Jets*

Clearly, it is unrealistic to assume that the outflow from GRB explosions will be uniform within some finite opening angle, outside which the Lorentz factor, γ, and energy per unit solid angle, ϵ, decrease very sharply (i.e., a top-hat jet). A more realistic situation is that the Lorentz factor (LF), the energy density, etc., are smooth functions of the angle, θ, from the jet axis, and possibly also of the distance, r, from the central source. The causality consideration suggests that the outflow is unlikely to be uniform over large angles, and moreover it provides a limit on how rapidly initial inhomogeneities can be smoothed out. Let the LF of the shell after elapsed time t since the explosion, measured in the lab frame, be $\gamma(t)$. The comoving time corresponding to this is $\sim t/\gamma$, and the distance traversed by sound waves during this

interval is $c_s t/\gamma \sim ct/3^{1/2}\gamma$. Therefore, the angular size of a causally connected region is $\sim 1/3^{1/2}\gamma$, and inhomogeneities on an angular scale of $\theta_{\rm ih} > \gamma^{-1}$, if present initially, will persist; the inhomogeneities can be smoothed out only when the LF has dropped below $\theta_{\rm ih}^{-1}$. As an example, the large angular scale inhomogeneities for a jet of opening angle 5° start to decrease only when the bulk LF has dropped below ~ 10, roughly 1 day after the explosion (as seen by the observer). It should also be noted that if one were to start with a uniform jet, or a top-hat profile for the LF or ϵ, the large gradient at the edge will decrease with time and the jet will develop angular structure (e.g., Granot et al. 2001).

The remainder of this section is devoted to the solution of the relativistic hydrodynamic equations to describe the evolution of jets from GRBs. The starting point is with the relativistic fluid equations (e.g., Landau & Lifshitz 1959),

$$\mathbf{T}^{\mu\nu}_{;\nu} = 0, \quad \mathbf{T}^{\mu\nu} = wu^\mu u^\nu + p\mathbf{g}^{\mu\nu} , \tag{1}$$

where $\mathbf{T}^{\mu\nu}$ is the energy-momentum tensor for an ideal fluid, u^μ is the 4-velocity of the fluid, $\mathbf{g}^{\mu\nu}$ is the metric tensor, p is the pressure, and $w = \rho + e + p$ is the proper enthalpy density, where ρ and e are the proper rest mass density and internal energy density, respectively, and $c = 1$ in our units. We use a spherical coordinate system and assume the flow possesses axial symmetry about the z-axis, i.e., u^ϕ, $\partial/\partial\phi = 0$. Under these assumptions the t-, r-, and θ-components of equation (1) are

$$\frac{\partial}{\partial t}(w\Gamma^2 - p) + \frac{1}{r^2}\frac{\partial}{\partial r}(r^2 w\Gamma^2 v_r) + \frac{1}{r\sin\theta}\frac{\partial}{\partial\theta}\left(w\Gamma^2 v_\theta \sin\theta\right) = 0 , \tag{2}$$

$$\frac{\partial}{\partial t}(w\Gamma^2 v_r) + \frac{1}{r^2}\frac{\partial}{\partial r}(r^2 w\Gamma^2 v_r^2) + \frac{1}{r\sin\theta}\frac{\partial}{\partial\theta}(w\Gamma^2 v_r v_\theta \sin\theta) + \frac{\partial p}{\partial r} - \frac{w\Gamma^2 v_\theta^2}{r} = 0 , \tag{3}$$

$$\frac{\partial}{\partial t}(w\Gamma^2 v_\theta) + \frac{1}{r^2}\frac{\partial}{\partial r}(r^2 w\Gamma^2 v_r v_\theta) + \frac{1}{r\sin\theta}\frac{\partial}{\partial\theta}(w\Gamma^2 v_\theta^2 \sin\theta) + \frac{1}{r}\frac{\partial p}{\partial\theta} + \frac{w\Gamma^2 v_r v_\theta}{r} = 0 , \tag{4}$$

where v_r and v_θ are the r- and θ-components of the fluid velocity, and $\Gamma = (1 - v_r^2 - v_\theta^2)^{-1/2}$ is the Lorentz factor of the fluid. Assuming that pair production has a negligible effect on the rest mass density, baryon number conservation implies

$$(\rho u^\mu)_{;\mu} = \frac{\partial}{\partial t}(\rho\Gamma) + \frac{1}{r^2}\frac{\partial}{\partial r}(r^2\rho\Gamma v_r) + \frac{1}{r\sin\theta}\frac{\partial}{\partial\theta}(\rho\Gamma v_\theta \sin\theta) = 0 . \tag{5}$$

We assume an equation of state

$$p = (\hat\gamma - 1)e = \frac{\hat\gamma - 1}{\hat\gamma}(w - \rho) \quad \text{with} \quad \hat\gamma = \frac{4\Gamma + 1}{3\Gamma} . \tag{6}$$

Equations (2)–(6) can be solved together to determine the structure and evolution of the outflow from GRBs. The computation time, for a 1 GHz clock speed computer, a modest resolution of 100×1000 in the r- and θ-coordinates (to keep the error small in finite difference schemes), and 5000 time steps, is expected to take of order several hours to complete one run for one set of initial conditions; for comparison the two-dimensional relativistic jet hydrodynamics calculation of Miller & Hughes, reported in Granot et al. (2001), took several hours to days of computation time, for low- to medium-resolution runs, to follow the evolution for $\gtrsim 10$ observer days, while an even longer computational time was required for the higher resolution runs. The successful modeling of light curves of a single GRB to determine various parameters requires several thousand runs, and thus the computation time to model one GRB, using a two-dimensional code, is currently estimated to range from months to years. Using many processors simultaneously can help reduce the actual overall time required, but at any rate, this requires a great computational effort.

The computation time can be drastically decreased by reducing the problem to a one-dimensional system by integrating out the radial dependence for all the relevant variables over the width of the outflow plus the swept-up material. The physical motivation for this is that jets in GRBs are in fact thin shells.[2] This procedure reduces the computing time drastically without introducing a significant loss of information as far as the emergent synchrotron emission is concerned; we find that the light curves from a relativistic spherical shock that has radial structure described by the self-similar Blandford-McKee (1976) solution is almost the same as in a model in which the radial dependences have been integrated out and the shell thickness is taken to be zero (see Fig. 5 of Granot, Piran, & Sari 1999a).

The shock front is a two-dimensional surface described by $r = R(\theta, t)$. The shocked fluid is concentrated in a thin shell of thickness $\Delta R \sim R/4\Gamma^2 \ll R$ for a relativistic flow,[3] and therefore it makes sense to integrate all the dependent variables, such as p, w, Γ, etc., over the width of the shell in the radial direction. We define quantities averaged over r, at a fixed θ and lab frame time t, as follows:

$$\Pi = \int_0^R dr\, r^2 p , \quad \Pi\overline{\Gamma}^2 = \int_0^R dr\, r^2 p\Gamma^2 ,$$
$$\overline{\Gamma}\overline{u}_\theta\Pi = \int_0^R dr\, r^2 p\Gamma u_\theta , \tag{7}$$

$$\Pi\overline{\Gamma}\overline{u}_r = \int_0^R dr\, r^2 p\Gamma u_r , \quad \chi_1\Pi\overline{u}_r\overline{u}_\theta = \int_0^R dr\, r^2 p u_r u_\theta ,$$
$$\chi_2\overline{u}_\theta^2\Pi = \int_0^R dr\, r^2 p u_\theta^2 , \tag{8}$$

$$\mu_s \equiv \frac{dM_s}{d\Omega} = \int_0^R dr\, r^2\rho_s\Gamma , \quad \mu_0 \equiv \frac{dM_0}{d\Omega} = \int_0^R dr\, r^2\rho_0\Gamma , \tag{9}$$

where μ_s and μ_0 (ρ_s and ρ_0) are the rest mass per unit solid angle (proper rest mass density) of swept-up material and of the original ejecta, respectively, and χ_1 and χ_2 are dimensionless correlation coefficients of order unity magnitude, which are taken to be independent of time. Integration of equation (2) times r^2 over the radial interval corresponding to the width of the shell when the shell is located at $R(t)$ yields

$$\frac{\partial}{\partial t}(\xi\overline{\Gamma}^2 - \Pi) + \frac{1}{\sin\theta}\frac{\partial}{\partial\theta}\left(\frac{\overline{u}_\theta\overline{\Gamma}\xi\sin\theta}{R}\right) = \rho_{\rm ext}(R)R^2\frac{\partial R}{\partial t} , \tag{10}$$

[2] At a distance r from the center of the explosion, the laboratory frame radial thickness of the ejecta plus the swept-up shock-heated material moving with LF γ is $\sim r/4\gamma^2$, whereas its transverse dimension is $r\theta_j$. Therefore the geometric shape of the system is that of a thin disk as long as $\theta_j \gg 1/4\gamma^2$.

[3] In fact, even as the flow becomes nonrelativistic, we still expect $\Delta R/R \lesssim 0.1$, as in the Sedov-Taylor self-similar solution, so that the thin-shell approximation should still be reasonable.

where

$$\xi \equiv \frac{\mu_0 + \mu_s}{\overline{\Gamma}} + \frac{\hat{\gamma}}{\hat{\gamma} - 1}\Pi \,. \tag{11}$$

An integration of equations (3) and (4) over the width of the shell gives

$$\frac{\partial}{\partial t}\left(\xi\overline{\Gamma}\overline{u}_r\right) + \frac{\chi_1}{\sin\theta}\frac{\partial}{\partial\theta}\left(\frac{\overline{u}_\theta\overline{u}_r\xi\sin\theta}{R}\right) - \frac{\chi_2\xi\,\overline{u}_\theta^2}{R} - \frac{2\Pi}{R} = 0 \,, \tag{12}$$

$$\frac{\partial}{\partial t}\left(\xi\overline{\Gamma}\overline{u}_\theta\right) + \frac{\chi_2}{\sin\theta}\frac{\partial}{\partial\theta}\left(\frac{\overline{u}_\theta^2\xi\sin\theta}{R}\right) + \frac{\chi_1\xi\,\overline{u}_r\overline{u}_\theta}{R} + \frac{1}{R}\frac{\partial\Pi}{\partial\theta} = 0 \,, \tag{13}$$

and the closure relation, given below, is obtained by integrating the equation $\Gamma^2 = 1 + u_r^2 + u_\theta^2$, times the pressure p, over the width of the shell

$$\overline{\Gamma}^2 - \chi_3\overline{u}_r^2 - \chi_2\overline{u}_\theta^2 = 1 \,, \tag{14}$$

where $\chi_3 \approx 1$ is a constant factor and $\chi_3 = 1$ corresponds to the assumption that $1 - \overline{u}_r/\overline{\Gamma} \ll 1$.

In deriving these equations it was assumed that the ejecta moves with the shocked interstellar matter (ISM), i.e., that the radial and the transverse components of the ejecta velocity are the same as those of the swept-up ISM. Under this assumption the mass continuity equations for the ejecta and the shocked ISM, respectively, are

$$\frac{\partial\mu_0}{\partial t} + \frac{1}{\sin\theta}\frac{\partial}{\partial\theta}\left(\frac{\overline{u}_\theta\mu_0\sin\theta}{R\overline{\Gamma}}\right) = 0 \,, \tag{15}$$

$$\frac{\partial\mu_s}{\partial t} + \frac{1}{\sin\theta}\frac{\partial}{\partial\theta}\left(\frac{\overline{u}_\theta\mu_s\sin\theta}{R\overline{\Gamma}}\right) = \rho_{\rm ext}(R)R^2\frac{\partial R}{\partial t} \,. \tag{16}$$

The velocity of the shock front is given by the shock jump conditions (Blandford & McKee 1976):

$$v_{\rm sh} = \sqrt{1 - \frac{\hat{\gamma}(2-\hat{\gamma})(\Gamma_{\rm ps} - 1) + 2}{(\Gamma_{\rm ps} + 1)\left[\hat{\gamma}(\Gamma_{\rm ps} - 1) + 1\right]^2}} \,, \tag{17}$$

where $\Gamma_{\rm ps} \approx \bar{\Gamma}$ is the postshock LF. The shock jump conditions imply that in the rest frame of the fluid before the shock (which in our case is the lab frame) the direction of the velocity of the fluid just behind the shock is always perpendicular to the shock front. To propagate the shock front in time, we assume that the average velocity of the shocked fluid is a good approximation for its value just behind the shock and obtain

$$\frac{\partial R}{\partial t} = v_{\rm sh}\sqrt{1 + \left(\frac{\overline{u}_\theta}{\overline{u}_r}\right)^2} \,. \tag{18}$$

Equations (10)–(18) are solved numerically with appropriate initial conditions (discussed below), to determine the evolution of the jet.

2.2. *Initial and Boundary Conditions*

The initial conditions are chosen at a lab frame time t_0 after the internal shocks have ended and before there is a significant deceleration due to the sweeping up of the external medium. We implement a number of different initial conditions, one of which is that the initial energy (including the rest mass energy) per unit solid angle, ϵ, and the initial Lorentz factor (-1) are power-law functions of θ, outside a core of opening angle θ_c. The initial energy per unit solid angle, $\epsilon(\theta, t_0)$, and the LF for the power-law model, respectively, are

$$\epsilon(\theta, t_0) = \epsilon_0\Theta^{-a} \,, \quad \Gamma(\theta, t_0) = 1 + (\Gamma_0 - 1)\Theta^{-b} \,, \tag{19}$$

where ϵ_0 and Γ_0 are the initial energy per unit solid angle and Lorentz factor at the jet axis, respectively, and

$$\Theta \equiv \sqrt{1 + \left(\frac{\theta}{\theta_c}\right)^2} \,. \tag{20}$$

Another initial condition we explore is a Gaussian profile for which $\epsilon(\theta, t_0)$ and $\Gamma(\theta, t_0) - 1$ are proportional to $\exp(-\theta^2/2\theta_c^2)$. The Gaussian jet profile was mentioned in Zhang & Meszaros (2002); however, they did not calculate the jet dynamics or light curve for this case.

Equation (19), or its counterpart for the Gaussian case, are applied only as long as $\Gamma(\theta, t_0) > 1.1$. At larger angles, we assume a uniform outflow, the parameters of which are set by the continuity condition.

We assume that the velocity is initially purely in the radial direction, i.e.,

$$v_\theta(\theta, t_0) = 0 \,, \quad v_r(\theta, t_0) = \sqrt{1 - \Gamma^{-2}(\theta, t_0)} \,, \tag{21}$$

while the initial radius is given by $R(\theta, t_0) = t_0 v_r(\theta, t_0)$.

The angular derivative of all dependent variables except $\overline{u}_\theta$ is zero at the pole and the equator, whereas $\partial\overline{u}_\theta/\partial\theta$ at the pole is determined by the assumption of axisymmetry, and at the equator by the reflection symmetry; $\overline{u}_\theta$ vanishes at the pole and at the equator.

2.3. *Numerical Results*

Equations (10)–(18) are solved using the two-step Lax-Wendroff scheme, to determine the evolution of the jet, for several different choices of initial conditions. The number of grid points in the angular directions is taken to be about 2000, and the time step is chosen to satisfy the Courant condition. The numerical solution respects global energy conservation to within 0.1%. We have looked into the dependence of the solution on the value of the dimensionless correlation parameters χ_1 and χ_2 and find consistent solutions for χ_1 between 0.8 and 1, and χ_2 approximately between 0.9 and 1.2. Outside this range of parameters the code is unstable and the solution unphysical, and the energy conservation is not satisfied. Inside this range the solution is not sensitive to the exact value of χ_1 and χ_2.

The evolution of $\overline{\Gamma}(\theta)$, $\overline{u}_\theta(\theta)$, and $\epsilon(\theta)$ are shown in Figures 1–4 for $(a, b) = (0, 2)$, $(2, 0)$, and $(2, 2)$, and for a Gaussian jet. Note that the transverse velocity in the comoving frame of the shocked fluid, $v'_\theta = \overline{u}_\theta$, is much less than the sound speed, $3^{-1/2}$, throughout much of the time and approaches the sound speed only when the jet Lorentz factor on the axis has fallen to a value of order a few. Clearly, this result depends on the gradient of the initial LF or ϵ at the initial time, and therefore the transverse velocity is found to be largest for the Gaussian case, which has the highest gradient of all the models we have considered.

The small value for v'_θ can be understood from equation (13). Ignoring the second-order term in $\overline{u}_\theta$ and noticing that the "source term" for $\overline{u}_\theta$ is the gradient of Π, we find that $\overline{u}_\theta \sim (\overline{\Gamma}\delta\theta)^{-1}$, where $\delta\theta$ is the angular scale for the variation

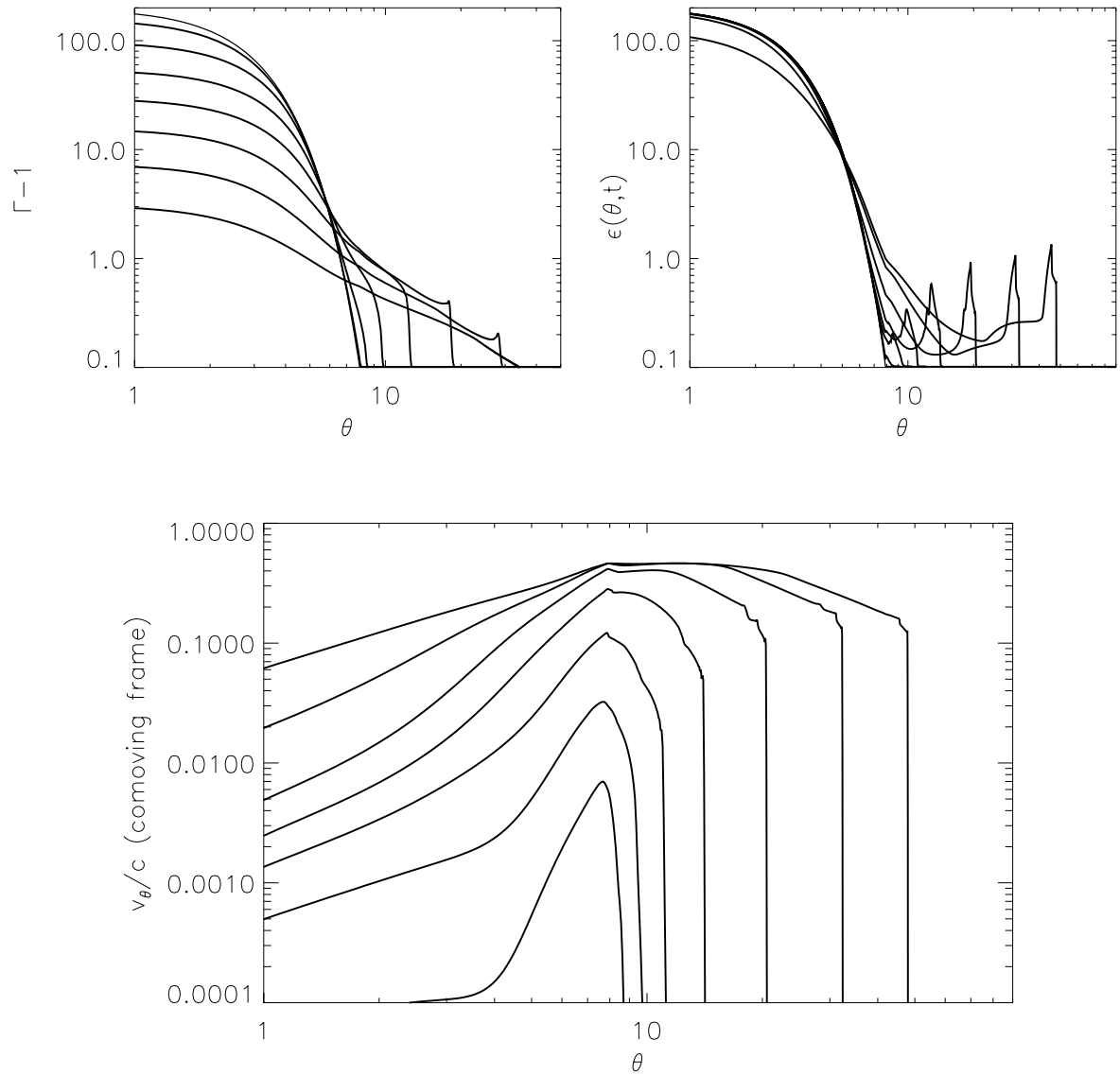

FIG. 1.—Different panels show the evolution of the Lorentz factor, $\overline{\Gamma}(\theta, t)$, the energy per unit solid angle, $\epsilon(\theta, t)$, and the transverse velocity in the comoving frame, $v'_\theta/c = \overline{u}_\theta$, for a jet with an initially Gaussian profile, i.e., $\overline{\Gamma}$ and ϵ proportional to $\exp(-\theta^2/2\theta_c^2)$ at the initial time. The parameters are $\theta_c = 0.035$ rad, $\epsilon(\theta = 0, t_0) = 10^{53}/4\pi$ ergs sr^{-1}, $\overline{\Gamma}(\theta = 0, t_0) = 200$, and the density of the external medium is 10 particles per cubic centimeter. At angles larger than about 6°.5 when $\overline{\Gamma}$ drops below 1.1, the LF and ϵ are taken to be independent of θ. Note that the energy per unit solid angle does not change much with time except at large angles where it was small initially, and we see it increase with time. *Bottom*, Sideways expansion of the jet showing the edge of the "relativistic jet," i.e., the vertical line where the transverse velocity drops to zero, which is moving to larger angles with time; *top*, jet edge and its motion, appearing as a sharp drop in $\Gamma - 1$. The sharp jump in the lateral velocity and energy density may be understood as a formation of a shock wave in the lateral direction. The numerical scheme we use becomes unstable when $\overline{\Gamma}$ drops below 4 at $\theta = 0$ or v_θ/c becomes larger than about 0.4; the LF near the edge of the jet is close to 1.01 when the code becomes unstable. It should be noted that the transverse velocity depends on the gradient of the energy density in the transverse direction and on the value of LF locally and not along the jet axis. And so our result for the transverse velocity, that it remains below the sound speed throughout much of the jet evolution, is not compromised by the numerical instability. The lab frame time increases monotonically from the curve with smallest v_θ/c to the curve with highest v_θ/c (*bottom*), and the time increases from the highest to the lowest curves (*top*).

of Π or the energy density. Thus, we get an appreciable transverse velocity in the comoving frame only when $\overline{\Gamma}\delta\theta \lesssim 1$.

Another way of deriving this result is from the shock jump conditions, which imply that the velocity, $\boldsymbol{v}_{\rm ps}$, of the fluid just behind the shock in the rest frame of the fluid before the shock (the lab frame in our case) is perpendicular to the shock front. This implies that the angle α between $\hat{\boldsymbol{v}}_{\rm ps}$ and $\hat{\boldsymbol{r}}$ (i.e., $\hat{\boldsymbol{v}}_{\rm ps} \cdot \hat{\boldsymbol{r}} = \cos\alpha$) satisfies

$$\tan\alpha = \frac{v_\theta}{v_r} = -\frac{1}{R}\frac{\partial R}{\partial \theta}\,. \tag{22}$$

For a relativistic flow $v_\theta < \Gamma^{-1} \ll 1$ so that $v_\theta \ll v_r \approx 1$ and $\alpha \approx \tan\alpha \approx v_\theta$. Thus we have $v_\theta \approx -\partial \ln R/\partial\theta$, and since $R \approx (1 - 1/2\Gamma^2)t$, this implies $v_\theta \approx -\Gamma^{-3}\partial\Gamma/\partial\theta$, or $v_\theta \sim 1/(\Gamma^2\delta\theta)$ and $u_\theta = \Gamma v_\theta \sim 1/(\Gamma\delta\theta)$, where $\delta\theta$ is the angle over which Γ varies appreciably. Therefore, this reproduces the result of the previous paragraph, as it is easy to show that the angular scales for the variation of Π and Γ are similar. From the definition of Π (eq. [7]), we have $\Pi \sim pR^2\Delta R \sim pR^3/4\Gamma^2$, and since the shock jump conditions imply $3p = e = 4\Gamma^2\rho_{\rm ext}(R)$, this gives $\Pi \sim \rho_{\rm ext}(R)R^3/3$, i.e., Π is a power law in $R \approx (1 - 1/2\Gamma^2)t$ and therefore varies over the same angular scales as Γ. The transfer of energy

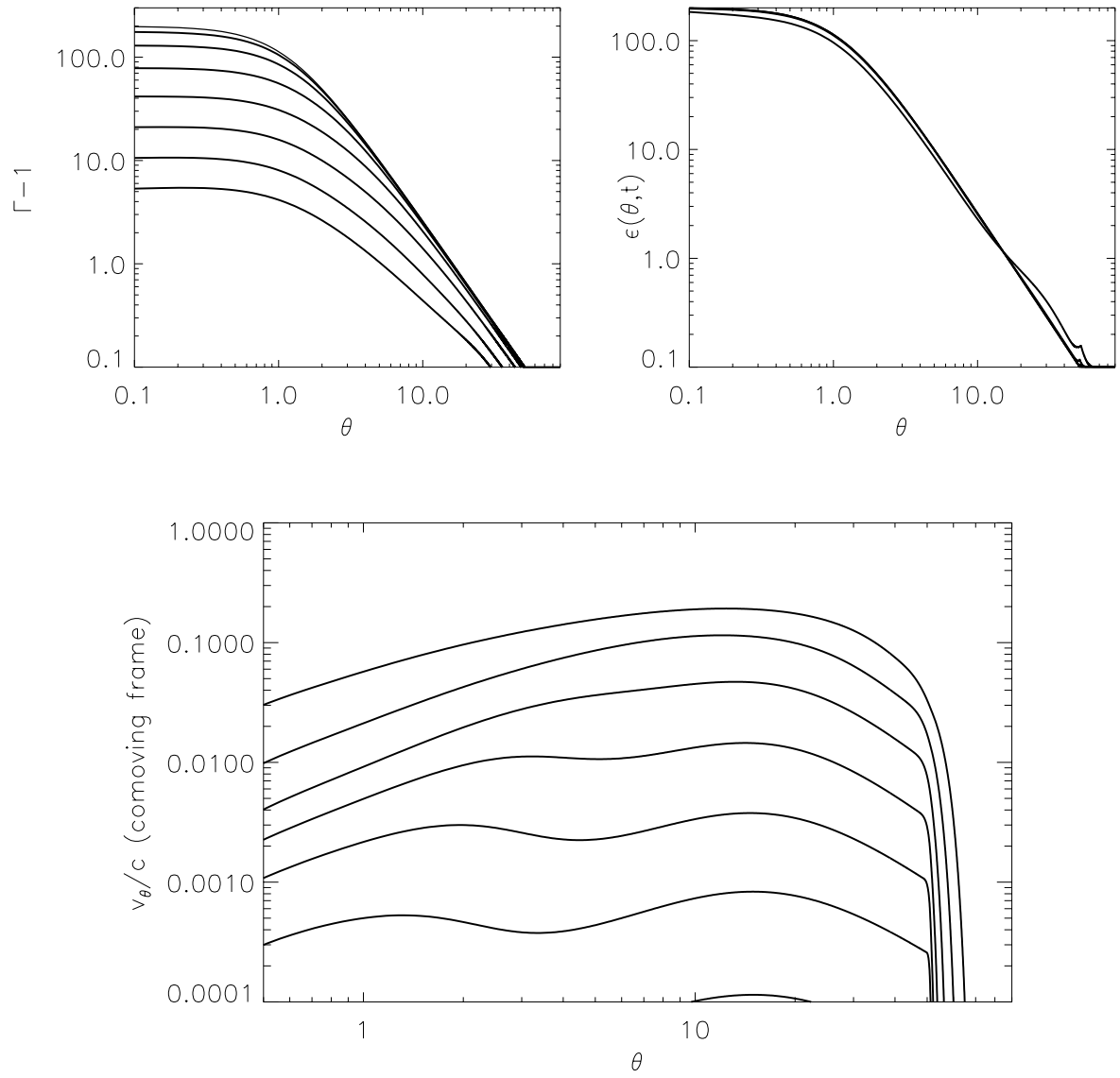

FIG. 2.—Evolution of the Lorentz factor $\overline{\Gamma}(\theta, t)$, the energy per unit solid angle, $\epsilon(\theta, t)$, and the transverse velocity in the comoving frame, $v'_\theta/c = \overline{u}_\theta$, for a jet with initial $\overline{\Gamma} = 1 + 199/(1 + \theta^2/\theta_c^2)$ and $\epsilon = \epsilon_0(1 + \theta^2/\theta_c^2)^{-1}$ with $\epsilon_0 = 10^{53}/4\pi$ ergs sr^{-1} and $\theta_c = 0.02$ rad; this initial profile corresponds to $a = 2$ and $b = 2$ in the notation of eq. (19). The density of the external medium is 10 particles per cubic centimeter. Note that the memory of the initial core angle, θ_c, is not erased with time, and in fact it remains unchanged until quite late times (*top left*). Moreover, the energy per unit solid angle does not change much with time either, except at large angles for which it was initially small, and we see it increase slightly with time. The transverse velocity v'_θ (*bottom*) remains quite small throughout much of the evolution of jet and even at late stages is about a factor of 3 smaller than the sound speed; the oscillations seen at early time in v_θ are almost certainly unphysical and numerical in origin.

from small to large angles over the course of the evolution of the jet, from a highly relativistic to a mildly relativistic regime, is also found to be small (Fig. 3).

The Gaussian initial jet profile is a smooth and more realistic version of a top-hat jet, in which the hydrodynamic quantities are roughly constant within some typical opening angle and sharply drop outside this angle (though they drop smoothly, not in a step function as in the top-hat jet). We therefore expect the results for an initial Gaussian profile to be similar to those of an initial top-hat jet profile. The hydrodynamic evolution of the latter has been investigated using a two-dimensional hydrodynamic simulation (Granot et al. 2001) and was found to be quite similar to our results, namely, the lateral spreading of the jet was much smaller than the prediction of simple top-hat jet models, and there was very little lateral transfer of energy. The fact that our hydrodynamic results for an initial Gaussian profile are similar to the results of two-dimensional hydrodynamic simulations of an initial top-hat jet profile is very reassuring and gives us some confidence in our numerical scheme.

3. LIGHT CURVES

Once the jet dynamics and the pressure and density of the shocked fluid are known, the synchrotron plus inverse Compton emissions are calculated from the fractional energies contained in the magnetic field and relativistic electrons, which are parameterized by dimensionless numbers ϵ_B and ϵ_e, respectively. The electrons are assumed to be accelerated to a power-law distribution of energies, $dN/d\gamma_e \propto \gamma_e^{-p}$, promptly behind the shock, and then cool because of radiative losses and adiabatic cooling. The local

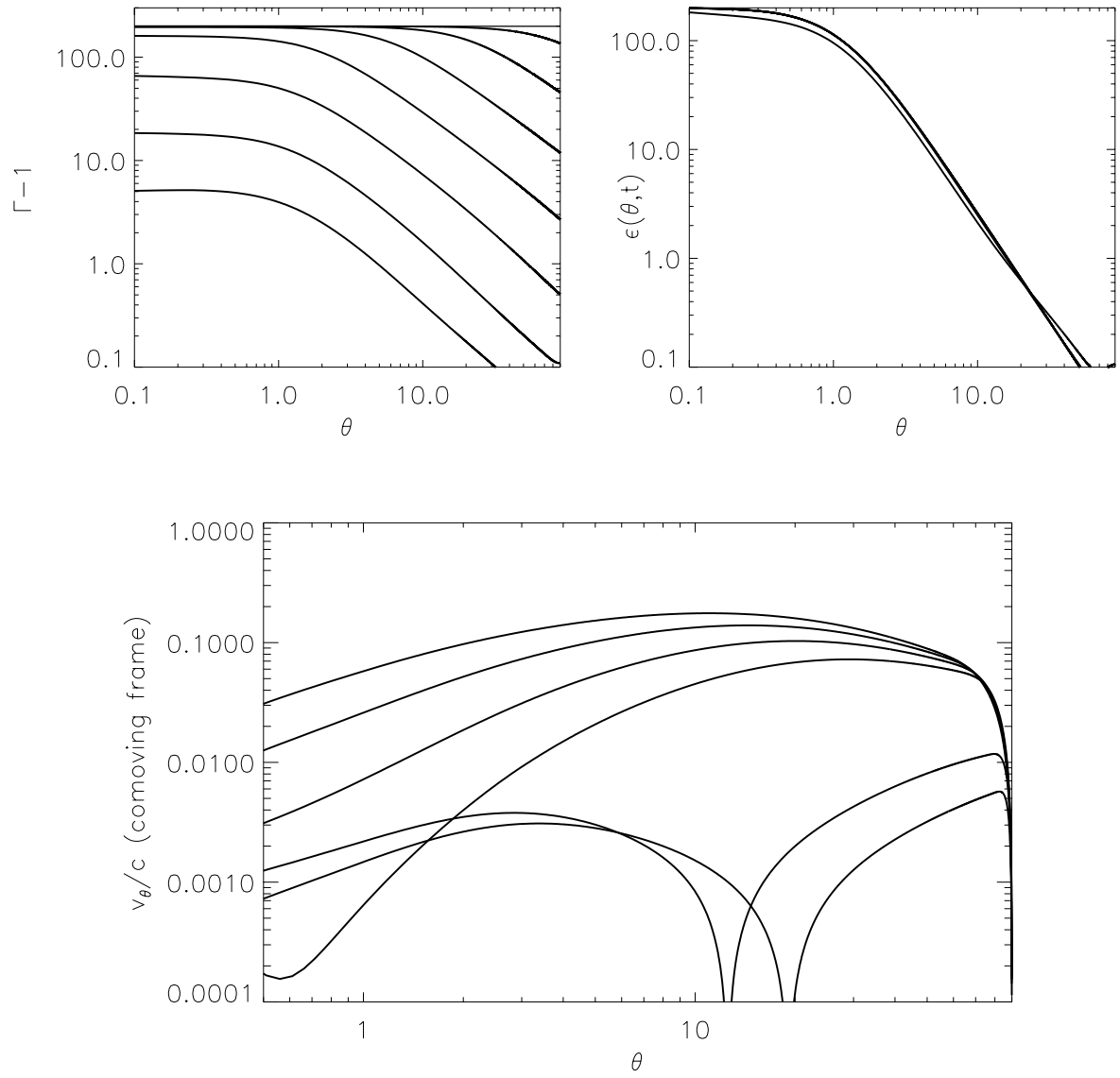

FIG. 3.—Same as Fig. 2, except that $a = 2$ and $b = 0$, i.e., initially $\epsilon = \epsilon_0(1 + \theta^2/\theta_c^2)^{-1}$ and $\overline{\Gamma}(\theta, t_0) = 200$, with $\theta_c = 0.02$ rad. See Fig. 2 legend for other details. The minimum in v_θ at early times (*bottom*; two lower curves) is because v_θ is changing sign from negative values at small angles to positive values at larger angles, and we have plotted $|v_\theta|$. The reason for the negative velocity near the jet axis at early times is that in this model the deceleration time is largest at the pole [$R_{\rm dec}$, $t_{\rm dec} \propto \Theta^{-2/3} = (1 + \theta^2/\theta_c^2)^{-1/3}$]; thus the pressure integrated over the shell thickness is close to zero at the pole and nonzero at large θ at times much less than the deceleration timescale at the pole. In this case a poleward transverse flow ensues. At $\theta > \theta_{\rm dec}(t)$ the $\epsilon \propto \Theta^{-2}$ profile dominates and induces a flow toward larger θ. At a later time, much greater than the deceleration time at the pole, the pressure integrated over the shell thickness is largest at the pole and the transverse velocity becomes positive everywhere. For the $(a, b) = (2, 1)$ model, for which $R_{\rm dec}$and $t_{\rm dec}$ are independent of θ, the transverse velocity is everywhere positive at all times as expected from this argument (we have verified this numerically).

emissivity, $j'_{\nu'}$ (the energy emitted per unit volume per unit time, frequency, and solid angle in the comoving frame), is approximated by a broken power law, with breaks at the cooling frequency, ν'_c, the synchrotron frequency, ν'_m, and the self-absorption frequency, $\nu'_{\rm sa}$.

Because of the curvature of the jet surface and its motion, photons arriving at some observed time $t_{\rm obs}$ were emitted at different spacetime points ($\boldsymbol{r}$, t). The calculation of afterglow multiwavelength light curves takes into account appropriate integration over equal arrival time surface as given by the following equation for the flux density:

$$F_\nu(t_{\rm obs}, \hat{\boldsymbol{n}})\delta t_{\rm obs} = \frac{(1+z)^2}{d_L^2} \frac{j'_{\nu'}(\boldsymbol{r}, t) d^4x}{\Gamma^2(\boldsymbol{r}, t)[1 - \boldsymbol{v} \cdot \hat{\boldsymbol{n}}]^2}, \quad (23)$$

where prime denotes quantities in the comoving frame of the fluid, $\hat{\boldsymbol{n}}$ is the direction to the observer (in the lab frame), ν' is related to the observed frequency ν by the Doppler shift relation, i.e., $\nu' = \nu(1 + z)\gamma(1 - \boldsymbol{v} \cdot \hat{\boldsymbol{n}})$, z and d_L, respectively, are the redshift and luminosity distance of the burst, and d^4x is the Lorentz invariant four-volume element. The observer time $t_{\rm obs}$ is related to the lab frame time t and location of the source $\boldsymbol{r}$ by $t_{\rm obs} = t - \boldsymbol{r} \cdot \hat{\boldsymbol{n}}$, with $\boldsymbol{r} \cdot \hat{\boldsymbol{n}} = r(\cos\theta \cos\theta_{\rm obs} + \sin\theta \sin\theta_{\rm obs} \cos\phi)$.

The light curves for the four jet profiles described in § 2.3 are shown in Figure 5, and the microphysics parameters for the shocked gas can be found in the figure legend. The average thermal Lorentz factor of shock-heated protons is given by $\overline{\Gamma}_{\rm th}(\theta, t) = 1 + \hat{\gamma}\Pi(\theta, t)/[\mu_s(\theta, t)(\hat{\gamma} - 1)] - \Pi/(\overline{\Gamma}^2\mu_s)$,

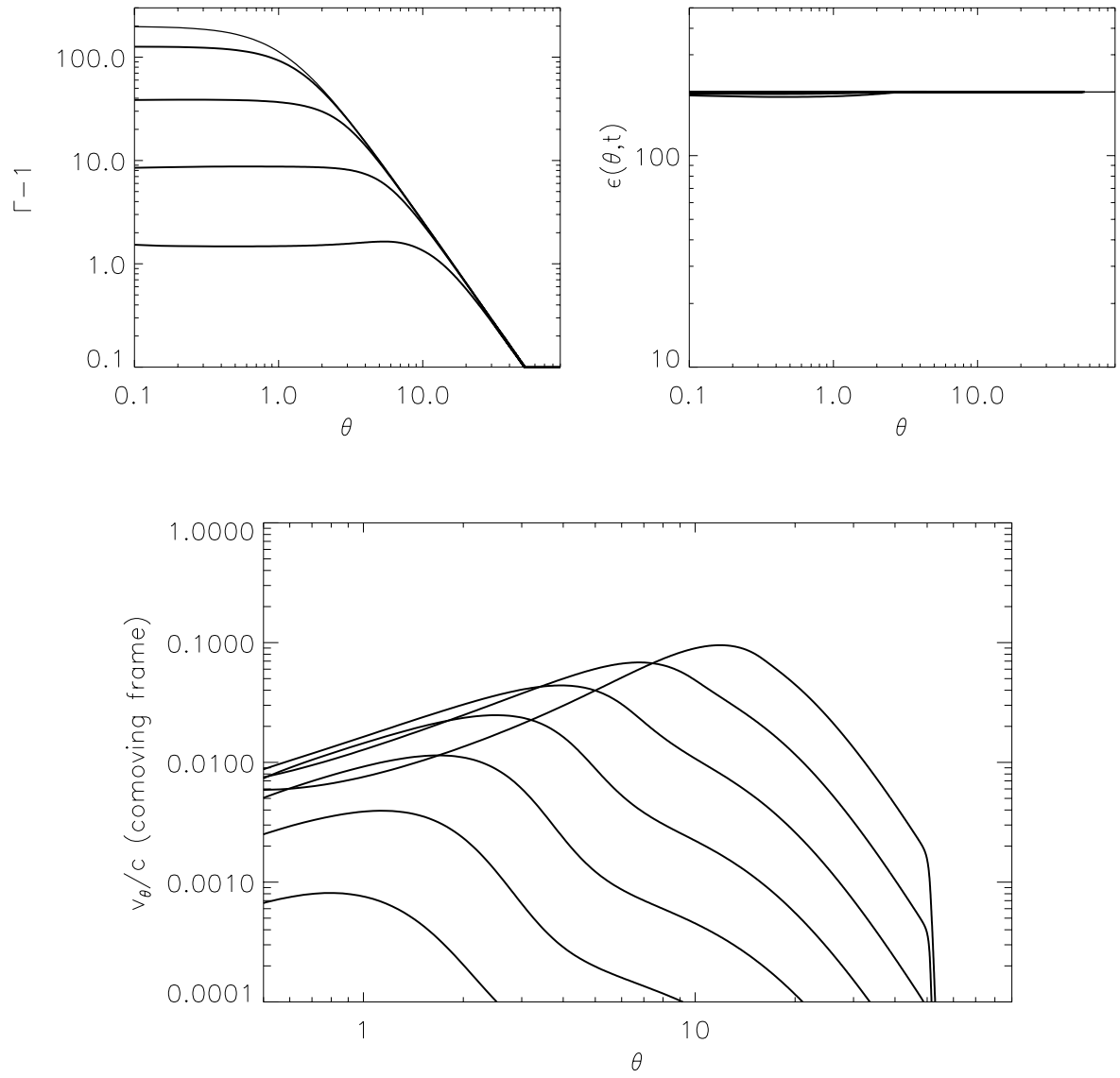

FIG. 4.—Same as Fig. 3, except that $a = 0$ and $b = 2$, i.e., initially $\epsilon(\theta, t_0) = 10^{53}/4\pi$ ergs sr^{-1}, and $\overline{\Gamma} = 1 + 199/(1 + \theta^2/\theta_c^2)$, with $\theta_c = 0.02$ rad. See caption of Fig. 2 for other details. Note that the jet becomes increasingly spherically symmetric with time in this case; Γ is independent of θ up to an angle at which shell deceleration has occurred, as in fact we expect when ϵ is independent of angle.

which turns out to be in very good agreement with the value one obtains from shock jump conditions.

The light curves for the Gaussian profile are rather similar to those for a top-hat jet, although the jet break for on-axis observers ($\theta_{\rm obs} \lesssim \theta_c$) is somewhat less sharp for the Gaussian profile, compared with a top-hat jet. The jet break, however, is still sufficiently sharp to be consistent with afterglow observations in most cases.

For $a = 0$ and $b = 2$, the energy per unit solid angle (ϵ) is independent of θ, so that after the deceleration time, $t_{\rm dec}$, the light curves for viewing angles, $\theta_{\rm obs} < \theta_{\rm dec}$, become the same as for a spherical flow with energy $4\pi\epsilon$; note that for this jet model $t_{\rm dec} \propto \Gamma^{-8/3} \propto \theta_{\rm obs}^{16/3}$ and $\theta_{\rm dec} \propto t_{\rm obs}^{3/16}$. These light curves do not show a jet break and are therefore not compatible with afterglow light curves that have a break.

For $a = 2$ and $b = 0$ (i.e., $\epsilon \propto \Theta^{-2}$ and $\Gamma = $ const, at initial time), there is a clear jet break for $\theta_{\rm obs} \gtrsim 2\theta_c$. The reason for this is that in this case much of the observed flux comes from small angles around the line of sight and the sharp break results when $\Gamma \lesssim \theta_{\rm obs}^{-1}$. For $\theta_{\rm obs} \gtrsim 7\theta_c$ there is a flattening of the light curve just before the jet break, due to the contribution from the inner parts of the jet, which is not seen in the observational data. This feature provides some constraint on this jet model and is discussed in Granot & Kumar (2003).

For $a = b = 2$ (i.e., ϵ, $\Gamma \propto \Theta^{-2}$ initially) the temporal decay slope before the jet break is steeper for small $\theta_{\rm obs}$ and more moderate for large $\theta_{\rm obs}$, and the magnitude of the increase in the slope after the steepening of the light curve is larger for larger $\theta_{\rm obs}$. If such a correlation is found in the data, it would provide support for this jet profile. The jet break is smoother for small $\theta_{\rm obs}$ and sharper for large $\theta_{\rm obs}$, making it difficult to explain the sharp jet breaks and small inferred $\theta_{\rm obs}$ (or opening angles for top-hat jets) that have been observed in quite a few afterglows.

It can be seen that for $a = b = 2$ and a small Γ_0 ($\sim$200 or less), the deceleration time, $t_{\rm dec}$, is quite large for large viewing angles, so that the light curve has a rising part at $t < t_{\rm dec}$

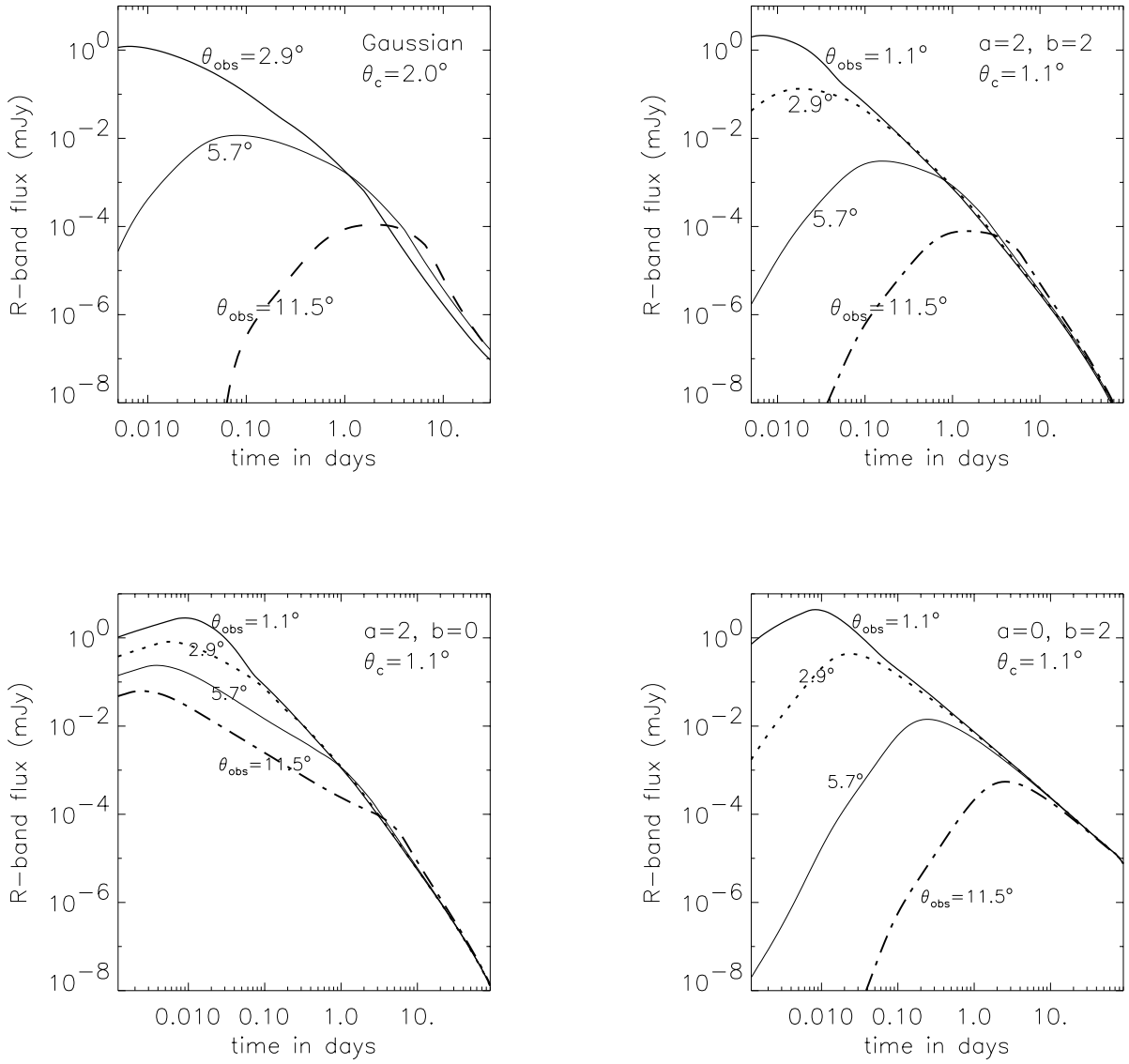

FIG. 5.—Observed *R*-band light curves for different viewing angles, θ_{obs}, with respect to the jet axis for the four jet profiles presented in Figs. 1–4. The basic jet model parameters are shown at top right in each panel (see eq. [19] for the definition of a and b). The remaining model parameters are the same for all panels: $z = 1$, the energy fractions in electrons and magnetic field, respectively, are $\epsilon_e = 0.5$ and $\epsilon_B = 10^{-4}$, the power-law index for electron distribution $p = 2.5$, and a constant external density $n = 10$ cm^{-3}. The light curves were calculated using the hydrodynamic simulation results shown in Figs. 1–4 (see appropriate figure captions for the details of the jet models) and eq. (23). For $a = b = 2$ the temporal decay slope before the jet break is more moderate for large θ_{obs}, and if Γ_0 is not very large (200 in this figure) then the deceleration time for large θ_{obs} is rather large. For $a = 2$ and $b = 0$ the jet break is rather sharp (as seen in observations), but at $\theta_{obs} \gtrsim$ a few, θ_c there is a flattening of the light curve just before the jet break (which is not seen in observations).

(Fig. 5). The fact that this is not seen in afterglow observations provides a lower limit on Γ_0 or an upper limit on b and thus can be used to constrain the structure of the jet. A more detailed analysis of the constraints that can be put on the jet profile from comparison to afterglow observations is discussed in an accompanying paper (Granot & Kumar 2002).

The light curves obtained for the hydrodymanic simulation of jets can be reproduced, quantitatively, by one or both of two simple and extreme models, which are described below. For more details on these models and their results we refer the reader to Granot & Kumar (2003). The two different simple models are referred to as model 1 and model 2.

In model 1, the energy per unit solid angle is assumed to retain its initial distribution, $\epsilon(\theta, t) = \epsilon(\theta, t_0)$. This represents the limiting case in which there is very little lateral transport of energy. Model 2 attempts to make the opposite assumption, that is, it assumes the maximal averaging of ϵ over the angle θ that is consistent with causality. The latter is achieved by averaging ϵ over its initial distribution, over the range in θ out to which a sound wave could have propagated from the initial time t_0. These two extreme assumptions are designed to bracket the expected range of possible behaviors for lateral energy transport. They are therefore expected to roughly cover the range of observed flux that a more rigorous treatment of the jet dynamics should give. In this sense they serve to quantify the uncertainties in the jet dynamics and light curves. For both models, the Lorentz factor is determined by energy conservation, i.e.,

$$\mu_0(\theta)\Gamma(\theta, t) + \mu_s(\theta, t)(\Gamma^2 - 1) = \epsilon(\theta, t) . \qquad (24)$$

4. CONCLUSION

We have carried out hydrodynamical simulations of a relativistic, collimated, axisymmetric outflow propagating into an external medium. For simplicity, we used a uniform density medium for the calculations presented in this work. However, the numerical scheme developed in this paper is good for any axially symmetric external density distribution (including power laws with the distance from the source, etc.). We have reduced the problem to a one-dimensional system of partial differential equations by integrating over the radial thickness of the outflow at a fixed lab frame time, thereby greatly reducing the computation time. The hydrodynamical results were used to calculate the synchrotron emission and light curves for a variety of observer angles with respect to the symmetry axis.

The model for GRB jets described in this paper is both rigorous and requires a very reasonable computational time, thus making it a useful tool for the study of GRB afterglows. In particular, it can be used in fits to afterglow observations, which can help constrain the jet profile, the external density profile, and the microphysics parameters of collisionless relativistic shocks.

We find that for jets with smoothly varying energy per unit solid angle and Lorentz factor, Γ, the maximum transverse fluid velocity in the comoving frame of the shocked fluid is typically substantially less than the speed of sound: the peak velocity is of order $1/(\Gamma\delta\theta)$, where $\delta\theta$ is the angular scale for the variation of the energy per unit solid angle, or of Γ. Thus large transverse velocities, approaching the sound speed, are realized only when the energy density varies rapidly with θ or Γ decreases to $(\delta\theta)^{-1}$. For the jet profiles examined in this paper, the largest lateral velocity occurred for the Gaussian profile, for which the initial gradients were largest. In fact, in this case a shock wave in the lateral direction develops because of the steep initial angular

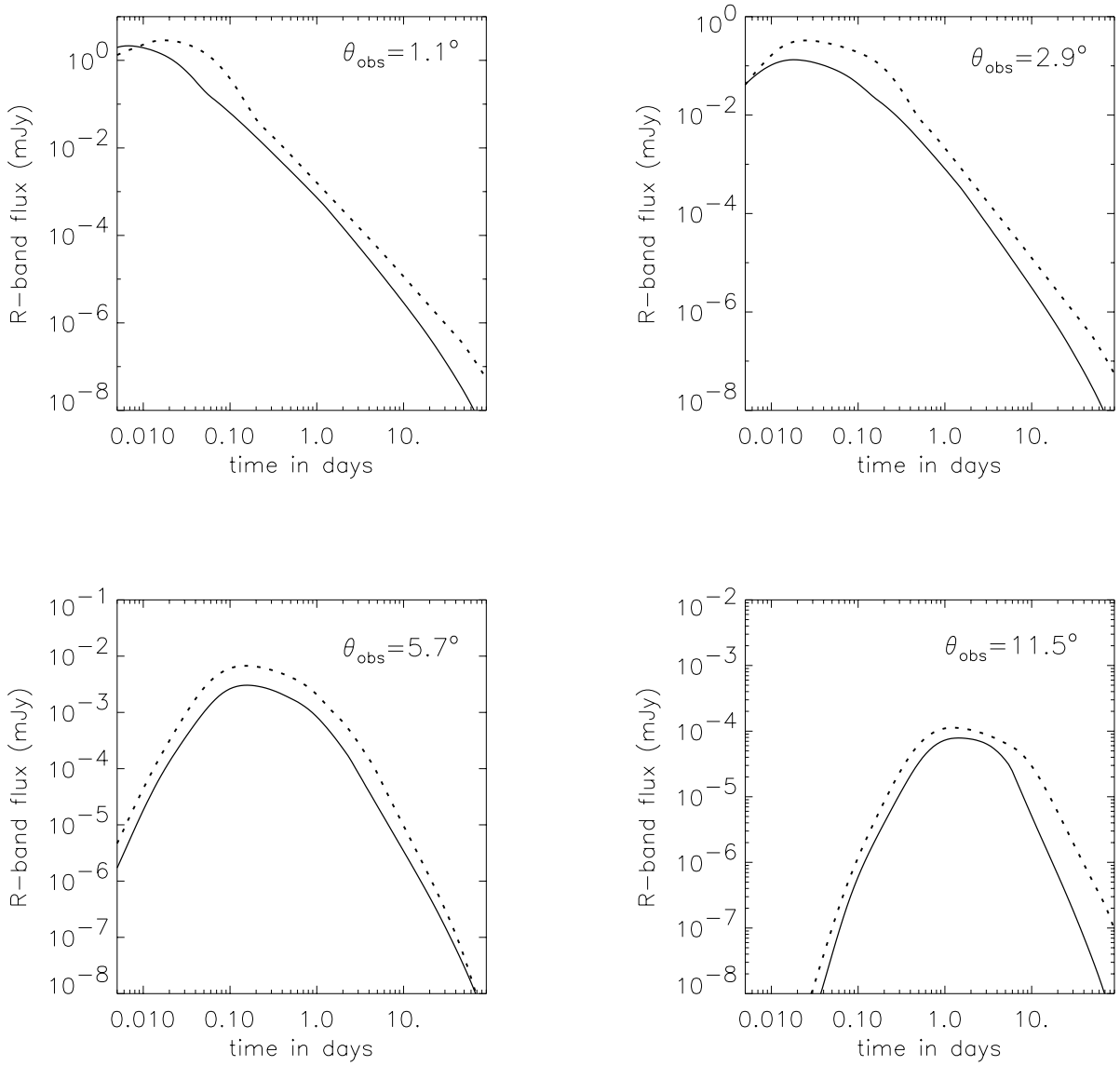

FIG. 6.—Comparison of light curves obtained with hydrodynamic simulation of jet (*solid line*) and a simple jet evolution model (*dotted curve*) in which the energy per unit solid angle is assumed to be time independent. The initial jet model is a power-law profile with $a = 2$, $b = 2$, and $\theta_c = 1.^\circ1$ (see eq. [19] for the definition of a, b, and θ_c), and the observer location with respect to the jet axis, θ_{obs}, is given in each panel. All the other parameters for the calculation are the same as in Fig. 5 (see the legend for details). For clarity the observed flux for the simple model has been multiplied by a factor of 2.

profile. This did not occur for the other jet profile, which had a more moderate angular dependence.

The energy per unit solid angle in the jet, ϵ, is found to change very slowly with time for all four of the jet models we have analyzed, and to a reasonable approximation ϵ can be considered essentially constant in time until Γ, along the jet axis, has dropped to ~ 4, which corresponds to about a week since the explosion in the observer frame (this is also the time when the transverse velocity is getting to be of order $0.2c$).

Therefore, a simple model in which the energy per unit solid angle is taken to be time independent and each element of the jet behaves as if it were part of a spherical flow with the same ϵ can serve as a useful approximation for the jet dynamics, as long as the jet is sufficiently relativistic. As can be seen from Figure 6, this simple model indeed seems to reproduce the light curves obtained using the hydrodynamical simulations quite well. However, the simple model must necessarily break down when the transverse velocity becomes of order c and the energy density is no longer constant. Unfortunately, this is also the regime when our hydrodynamical calculation becomes unstable.

We have calculated the observed light curves in the R band for several different jet angular profiles and viewing angles. We find that the light curves for a Gaussian jet profile are similar to those for a top-hat jet (as expected) and compatible with most observed jet breaks. The light curves for a jet with a constant energy per unit solid angle, ϵ, but $\Gamma(t_0)$ decreasing with θ, are similar to those for a spherical explosion and thus not applicable to cases in which we see a jet break in the light curve. For jet profiles in which initially $\epsilon \propto \Theta^{-2}$ and Γ is either constant or $\propto \Theta^{-2}$ do produce jet breaks in the light curves and have the advantage that these models can reproduce the "observed" narrow range for the total energy in GRB relativistic outflows (Panaitescu & Kumar 2002; Piran et al. 2001). A companion paper (Granot & Kumar 2003) discusses some preliminary constraints on jet profiles from qualitative comparison with observations.

J. G. thanks the support of the Institute for Advanced Study, funds for natural sciences.

REFERENCES

Blandford, R. D., & McKee, C. F. 1976, Phys. Fluids, 19, 1130
Chevalier, R. A., & Li, Z.-Y. 2000, ApJ, 536, 195
Frail, D., et al. 2001, ApJ, 562, L55
Granot, J., & Kumar, P. 2003, ApJ, 591, 1086
Granot, J., Panaitescu, A., Kumar, P., & Woosley, S. E. 2002, ApJ, 570, L61
Granot, J., Piran, T., & Sari, R. 1999a, ApJ, 513, 679
———. 1999b, ApJ, 527, 236
Granot, J., et al. 2001, in GRBs in the Afterglow Era, ed. E. Costa, F. Frontera, & J. Hjorth (Berlin: Springer), 312
Gruzinov, A. 1999, ApJ, 525, L29
———. 2001, ApJ, 563, L15
Königl, A., & Granot, J. 2002, ApJ, 574, 134
Kumar, P., & Panaitescu, A. 2000, ApJ, 541, L9
Landau, L. D., & Lifshitz, E. M. 1959, Course of Theoretical Physics: Fluid Mechanics (Vol. 6; Oxford: Pergamon Press)
Lipunov, V. M., Postnov, K. A., & Prokhorov, M. E. 2001, Astron. Rep., 45, 236
Medvedev, M. V., & Loeb, A. 1999, ApJ, 526, 697
Mészáros, P., Rees, M. J., & Wijers, R. A. M. J. 1998, ApJ, 499, 301
Moderski, R., Sikora, M., & Bulik, T. 2000, ApJ, 529, 151
Panaitescu, A., & Kumar, P. 2001a, ApJ, 554, 667
———. 2001b, ApJ, 560, L49
———. 2002, ApJ, 571, 779
Panaitescu, A., & Mészáros, P. 1999, ApJ, 526, 707
Piran, T. 1999, Phys. Rep., 314, 575
———. 2000, Phys. Rep., 333, 529
Piran, T., Kumar, P., Panaitescu, A., & Piro, L. 2001, ApJ, 560, L167
Price, P. A., et al. 2002,ApJ, 571, L51
Rhoads, J. 1999, ApJ, 525, 737
Rossi, E., Lazzati, D., & Rees, M. J. 2002, MNRAS, 332, 945
Sari, R., Piran, T., & Halpern, J. 1999, ApJ, 519, L17
Wijers, R. A. M. J., & Galama, T. J. 1999, ApJ, 523, 177
Zhang, B., & Mészáros, P. 2002, ApJ, 571, 876